

6-1-2007

Current-induced breakdown of carbon nanofibers

Makoto Suzuki

Yusuke Ominami

Quoc Ngo

Cary Y. Yang

Santa Clara University, cyang@scu.edu

Alan M. Cassell

See next page for additional authors

Follow this and additional works at: <https://scholarcommons.scu.edu/elec>

Recommended Citation

M. Suzuki, Y. Ominami, Q. Ngo, C.Y. Yang, A.M. Cassell, and J. Li, "Current-induced breakdown of carbon nanofibers," *Journal of Applied Physics* 101, 114307(5 pp) (2007). <https://doi.org/10.1063/1.2743086>

Copyright © 2007 American Institute of Physics Publishing. Reprinted with permission.

This Article is brought to you for free and open access by the School of Engineering at Scholar Commons. It has been accepted for inclusion in Electrical Engineering by an authorized administrator of Scholar Commons. For more information, please contact rsroggin@scu.edu.

Authors

Makoto Suzuki, Yusuke Ominami, Quoc Ngo, Cary Y. Yang, Alan M. Cassell, and Jun Li

Current-induced breakdown of carbon nanofibers

Makoto Suzuki,^{a)} Yusuke Ominami, Quoc Ngo, and Cary Y. Yang
Center for Nanostructures, Santa Clara University, Santa Clara, California 95053

Alan M. Cassell and Jun Li
NASA Ames Research Center, Moffett Field, California 94035

(Received 12 December 2006; accepted 13 April 2007; published online 7 June 2007)

We present a study of high-field transport in carbon nanofibers (CNFs) and breakdown phenomena due to current stress. *In situ* measurements with scanning transmission electron microscopy reveal that the failure mode of CNFs is strongly related to the morphology of graphite layers comprising CNFs. Comparison with carbon nanotube (CNT) breakdown is made, demonstrating that the current capacity of CNFs is described by a similar model as that of CNTs with a modification of the current capacity of each graphitic layer. The maximum current density is correlated with resistivity, leading to the conclusion that lower resistivity results in higher current capacity in CNFs. © 2007 American Institute of Physics. [DOI: 10.1063/1.2743086]

I. INTRODUCTION

Carbon-based nanostructures such as carbon nanotubes¹⁻⁴ (CNTs) and carbon nanofibers^{5,6} (CNFs) have been studied for high-performance devices and interconnects because of their chemically stable nature and high electrical and thermal conductivities.⁷ Recent progress in lowering the growth temperature of CNTs and CNFs has accelerated the development of potential applications.^{8,9} For on-chip interconnects²⁻⁴ and field-emitting devices,¹⁰ high-field transport is crucial for accurate device characterization and modeling. In the CNT system, unique phenomena have been observed under high electric field, including nonlinear transport property in single-walled CNTs¹¹⁻¹³ and a successive graphitic wall breakdown in multiwalled CNTs.¹⁴⁻¹⁷ In the CNF system, however, the high-field transport property has been reported only preliminarily.⁶ So far, much attention has been paid to the structural analysis of chemical vapor deposition (CVD)-grown CNFs using atomic-scale electron microscopy,¹⁸⁻²¹ revealing that CNFs consist of cup-shaped graphitic layers stacked along the fiber axis. Because of this morphology, electron transport in CNFs has an interlayer component where the electrons hop between graphitic layers. Thus we expect the structural damage due to high current stress to be different from those of CNTs.¹⁴⁻¹⁷ And analysis of the current-induced breakdown of CNFs is especially important for reliability considerations in interconnect applications.⁶

Here we report a systematic study of current-induced breakdown of CNFs and current-carrying capacity by means of *in situ* breakdown measurements with scanning transmission electron microscopy (STEM). We reveal that at high current stress, voids are created between graphitic layers and breakdown occurs along the cup-shaped graphitic layers. By comparing with CNT breakdown phenomena, a similar phenomenological model can be applied to CNFs with modified current capacity for each graphitic layer. A simple relation

between maximum current density and electrical resistivity is deduced, which shows that current-carrying capacity increases with decreased electrical resistivity.

II. EXPERIMENT

CNF samples are grown by plasma-enhanced chemical vapor deposition^{22,23} (PECVD) with a gas mixture of $\text{NH}_3:\text{C}_2\text{H}_2$ (4:1) at 4 Torr. The detailed growth condition is described elsewhere.²⁴ A 30 nm thick Ti adhesion layer is deposited on a Si substrate, followed by a 35 nm thick Ni catalyst layer deposited on Ti by ion beam sputtering. The structure of CNFs used in this study has been explored with STEM and characterized as exhibiting a cup-shaped morphology.^{21,25} Electrical measurements with concurrent STEM imaging are carried out in a field-emission scanning electron microscope with STEM capability using an electron beam energy of 30 keV (30 keV STEM, Hitachi S-4800). For CNF suspension and electrical measurement, an aluminum foil and a tungsten probe are placed in the 30 keV STEM specimen chamber with a separation of 5 μm , as

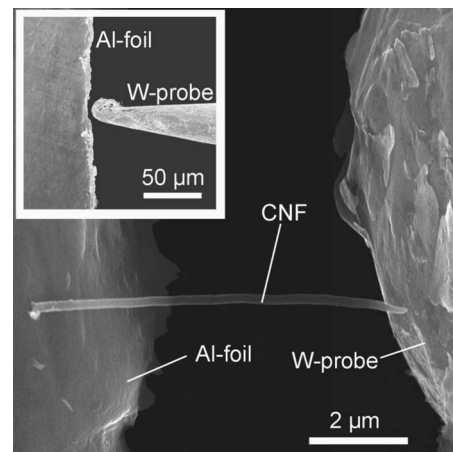


FIG. 1. A suspended CNF sample on 30 keV STEM holder. Inset: Wide view of electrode pair for breakdown experiment.

^{a)}Author to whom correspondence should be addressed; electronic mail: msuzuki@scu.edu

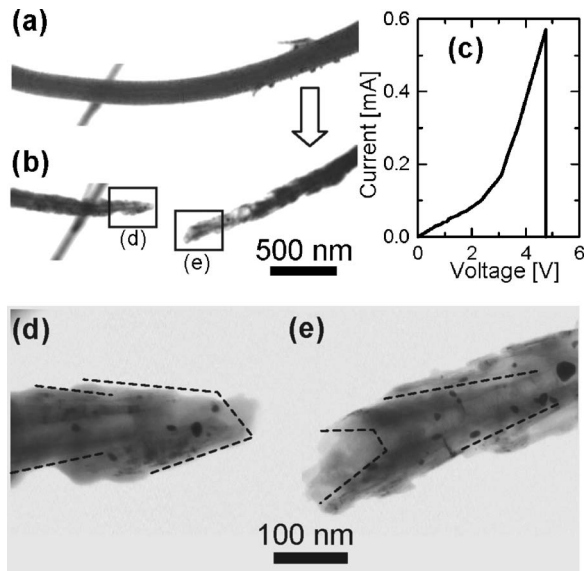


FIG. 2. Low-magnification STEM images of (a) an undamaged CNF and (b) failed CNF. (c) A current-voltage trace of the breakdown of the CNF shown in (a) and (b). (d) and (e) show the high-magnification images of failed ends in (b).

shown in the inset of Fig. 1. This makes the simultaneous acquisition of structural and electrical information possible. As-grown CNF samples are subjected to ultrasound agitation in an isopropyl alcohol solution following removal from the substrate and dispersed on this electrode pair. A CNF suspended between electrodes is shown in Fig. 1. All electrical measurements are performed under vacuum at 10^{-5} Torr. We have performed the breakdown experiment for 12 CNF samples, ranging from 60 to 240 nm in diameter. High-resolution STEM imaging is performed using a dedicated STEM with a beam energy of 200 keV (200 keV STEM, Hitachi HD-2300).

III. RESULTS

In Figs. 2(a) and 2(b), we show 30 keV STEM images of

a CNF before and after the current-induced breakdown, respectively. By passing current through the CNF, breakdown occurs near the midpoint at approximately 570 μ A and 4.8 V, as seen in the *I-V* trace of Fig. 2(c). The midpoint breakdown is consistent with diffusive transport observed in CNTs at a high bias,¹⁶ where electron-phonon scattering dominates.^{1,7} If we assume uniform radial current distribution in a CNF, the corresponding current density is 3×10^6 A/cm². The assumption of uniform radial current distribution requires a diffusive transport in a CNF. In the CNT system, end-contacted configuration of CNT-electrode interface needs to be realized to ensure that all graphitic walls make contact with the electrode.¹⁶ While our experiments of CNFs are carried out in a side-contacted configuration (Fig. 1), PECVD-grown CNF samples show diffusive transport²⁶ obeying Ohm's law; therefore it is valid to assume that all of the graphitic layers uniformly take part in electron transport. The failed ends of the CNF shown in Figs. 2(d) and 2(e) represent the cup-shaped morphology of graphitic layers. Dispersed Ni catalyst particles are also seen in broken fibers, showing that high-current stress raises the fiber temperature to above 1000 K and near the melting point of Ni particles.²⁷ The cup-shaped feature can be more clearly seen in another example of a partially failed CNF shown in Fig. 3(a). The damaged area of the CNF exhibits a steplike outer diameter, demonstrating that the graphitic layers are removed along the cup-shaped boundaries. The resulting damaged structure shows the stacked bundle of graphitic cups (5–20 nm thick), schematically shown in Fig. 3(a). In another CNF shown in Fig. 3(b), the cup-shaped end is not clear but graphitic layers become loose and voids are formed between them. High-resolution STEM images at 200 keV of a CNF with similar damage are shown in Figs. 3(c) and 3(d). The void structures created between graphitic layers are clearly observed. Also, graphitic layers are bundled mostly in 5–15 nm thick layers, as shown in Fig. 3(d).

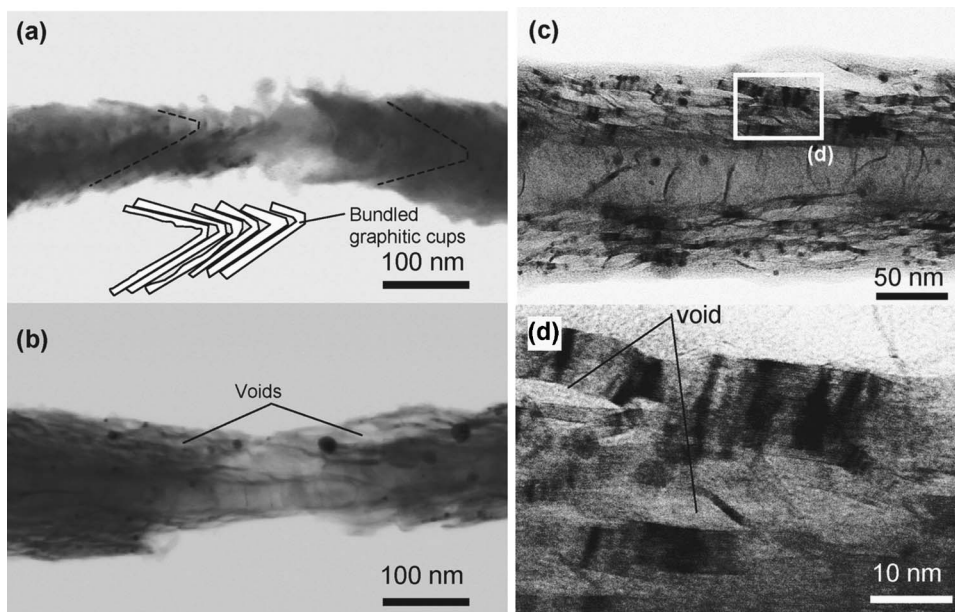


FIG. 3. (a) A partially failed CNF with cup-shaped failure. (b) A partially failed CNF with voids inside the body. [(c) and (d)] High-resolution 200 keV STEM images of a damaged CNF. Voids created between graphite bundles. The bundle structures can be seen with their width of 2–15 nm.

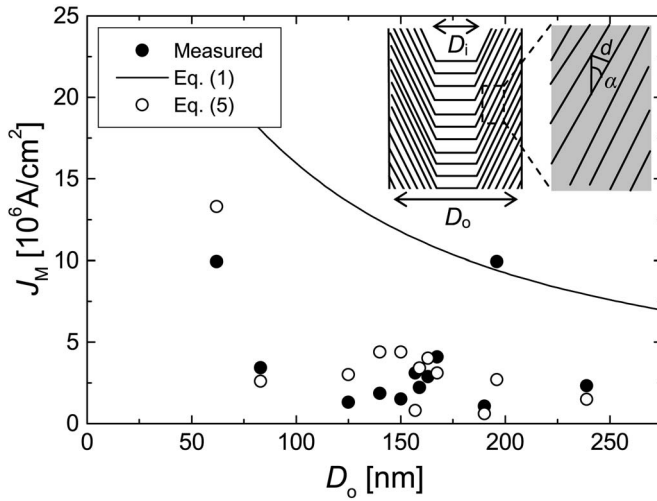


FIG. 4. Outer diameter dependence of measured maximum current density of CNFs (closed circles). The solid line represents the model of Eq. (1) with constant cone angle $\alpha=21^\circ$ based on CNT experiments (Refs. 14–17) and the open circles correspond to the estimated value using the model of Eq. (5) with resistivity correction. Inset: Schematic view of cup-shaped CNF.

IV. DISCUSSION

A. Structural damage

Both the cup-shaped failure and void creation observed in Fig. 3 can be explained by the relatively weak interlayer (layer-layer) bonding. The nanofiber tends to break up easily as a result of current stress, in contrast to CNT, where electron transport is strictly intralayer and strong bonds exist within each graphitic layer. From the observed bundle thickness and graphitic layer spacing of 0.34 nm, we estimate that 1 per 15–60 graphitic layers (<10%) has weak bonding. Thus the interlayer bonding strength is nonuniform, and some of the graphitic layers are weakly coupled with adjacent layers. This is possibly due to the fluctuation of the catalytic growth parameters, such as temperature, catalyst orientation, and a gas mixture.²⁸ The highly anisotropic thermal expansion coefficient of graphite single crystal²⁹ can also account for observed current-induced breakdown in CNFs. The larger thermal expansion coefficient in the direction normal to the graphitic layer accelerates the layer separation with resistive heating.

B. Diameter dependence of maximum current density

Figure 4 shows the relationship between observed maximum current density (J_M) and the CNF diameter (D_o) of 12 CNF samples (closed circles). With the exception of $D_o=60$ and 200 nm, most of the data points are distributed between $1 \times 10^6 \text{ A/cm}^2 < J_M < 5 \times 10^6 \text{ A/cm}^2$ without clear dependence on diameter. The average maximum current and current density are $670 \mu\text{A}$ and $3.6 \times 10^6 \text{ A/cm}^2$, respectively. In the case of CNTs,^{14–17} each graphitic wall can carry a current I_0 of 10–60 μA , above which the wall starts to be removed. A detailed measurement¹⁵ of I_0 shows that, for CNTs longer than 1 μm , I_0 is almost independent of its diameter and has an average value of around 20 μA . If we assume that this experimental observation can be applied to CNFs, we can derive the estimated maximum current by ac-

counting for the number of graphitic layers. As a first-order approximation, the structure of CNFs is characterized by outer diameter D_o , inner diameter D_i (bottom diameter of the graphitic cup), cone angle α , and interlayer spacing $d=0.34 \text{ nm}$, as shown in the inset of Fig. 4. This gives the total number of graphitic layers $N=(D_o-D_i)\cos\alpha/2d$ and maximum current $I_M=NI_0$. Thus, J_M is evaluated as

$$J_M = \frac{4NI_0}{\pi D_o^2}. \quad (1)$$

This leads to the average maximum current and maximum current density of $2060 \mu\text{A}$ and $1.2 \times 10^7 \text{ A/cm}^2$, respectively, even when considering the smallest value¹⁴ of I_0 , 12 μA . This is significantly larger than the observed value of $3.6 \times 10^6 \text{ A/cm}^2$ but is still much smaller than the current-carrying capacity of CNTs ($\sim 10^9 \text{ A/cm}^2$, Ref. 14). We plot the diameter dependence of the calculated curve of Eq. (1) in Fig. 4 with a solid line, assuming that α is a constant average value of 21° , while the observed values of α range from 5° to 50° . As can be seen, this curve predicts significantly larger current density than the observed data. This is expected since, as discussed above, CNFs have structural defects such as inhomogeneous interlayer bonding and dangling bonds at the periphery of cup-shaped graphite layers compared with the seamless CNT structure. A recent study on multiwall CNTs grown by thermal CVD process³⁰ with structural defects also shows reduced current capacity, consistent with our results.

To reproduce the observed J_M , we modify Eq. (1) by considering the reduction of current density due to resistive heating of CNFs. The temperature (T) distribution of one-dimensional conductor is described by the one-dimensional steady-state heat transport equation^{31,32}

$$\kappa \nabla^2 T - \gamma T + q = 0, \quad (2)$$

where κ , γ , and q are the thermal conductivity of the conductor, the thermal coupling with environment, and the generated heat per unit volume, respectively. The boundary conditions for Eq. (2) are that the temperature profile as well as its first derivative should be continuous at the CNF-electrode contacts. By assuming that the resistive heating is created only in the CNF, but not at the contacts, the maximum temperature at the middle of the CNF, $T(0)$, obtained from solving Eq. (2), is shown to be proportional to the generated heat density, $q=J^2\rho$, as follows:

$$T(0) = \frac{q}{\gamma} \left[1 - \exp\left(-\sqrt{\frac{\gamma L}{\kappa 2}}\right) \right], \quad (3)$$

where L is the CNF length between electrodes. Thus it is reasonable to consider that J_M is inversely proportional to the square root of resistivity, $J_M \propto \sqrt{T(0)/\rho}$, assuming that the current-induced breakdown is stimulated at a particular temperature. Since we use the value of I_0 from CNT experiments, this correction should be included for the modeling of CNFs. As shown in Ref. 26, electrical resistivity of CNFs can be evaluated by the anisotropic resistivity of bulk graphite as

$$\rho_{\text{CNF}} = \rho_a \cos^2 \alpha + \rho_c \sin^2 \alpha, \quad (4)$$

where $\rho_a = 4 \times 10^{-5} \Omega \text{ cm}$ and $\rho_c = 4 \times 10^{-2} \Omega \text{ cm}$ are resistivities along and perpendicular to the graphitic layers. Since ρ_c is three orders of magnitude larger than ρ_a , even a small cone angle can substantially increase resistivity. Using Eq. (4), Eq. (1) is modified as

$$J_M = \frac{4N}{\pi D_o^2} I_0 \sqrt{\rho_{\text{CNT}} / \rho_{\text{CNF}}}. \quad (5)$$

A CNT resistivity (ρ_{CNT}) of $1.9 \times 10^{-4} \Omega \text{ cm}$ derived in the similar experimental configuration¹⁷ is used. Note that the cone angle dependence of ρ_{CNF} in Eq. (5) is more prominent than the rather moderate angular dependence of N in Eq. (1), resulting in a substantial difference between CNFs and CNTs. We estimate J_M for all CNFs studied using Eq. (5), and plot them as open circles in Fig. 4. These calculated points are not aligned with a smooth curve since α is another variable in Eq. (5) through ρ_{CNF} . While several data points do not correctly reproduce the observed value, the overall trend of outer diameter dependence is well described. Indeed, the average J_M estimated by Eq. (5) is $3.6 \times 10^6 \text{ A/cm}^2$, consistent with experimental results. This result supports the assumption that the CNF breakdown is mainly governed by resistive heating. The difference between observed data and estimated J_M comes from the lack of the microscopic information on the defect density, defect types, and the inhomogeneous bonding nature of each sample, as shown in Fig. 3. This indicates that the reliable prediction of current capacity in CNFs is still difficult, while on average, maximum current density can be reasonably estimated using Eq. (5). This approach is contrasted with the analysis of current capacity in CNTs, where the tube length is the dominant parameter for current capacity.^{13,32,33} Our analysis is based on STEM observation that shows that the inner structure and breakdown process of CNFs vary between samples; thus current capacity can vary even when fiber lengths L are comparable ($L = 8 \pm 2 \mu\text{m}$).

C. Resistivity dependence of maximum current density

The results discussed in the previous section demonstrate that the effect of resistivity on current capacity is significant. In Fig. 5(a), the resistivity dependence of J_M is shown. Here, the resistivity is defined as the observed resistivity just prior to breakdown. The data exhibit clear correlation between resistivity and current capacity and can be described by a fitted power law relationship $J_M = A\rho^{-k}$, with $A = 2.7 \times 10^8$, $k = 0.58$, and ρ is in unit of $\mu\Omega \text{ cm}$. This strong dependence of J_M on electrical resistivity leads to the conclusion that lower electrical resistivity corresponds to higher current capacity. While the reliability of this fit measured by the square correlation coefficient (R^2) is relatively weak ($R^2 = 0.76$), the correlation can be improved in the following way. Figure 5(b) shows a different plot, J_M vs ρL , which is described again by a power law relationship $J_M = B(\rho L)^{-n}$, with $B = 2.1 \times 10^9$, $n = 0.68$, and ρL is in unit of $\mu\Omega \text{ cm } \mu\text{m}$. The fit is obtained with much improved R^2 value of 0.91; thus the J_M of our samples scales well with ρL , rather than ρ ,

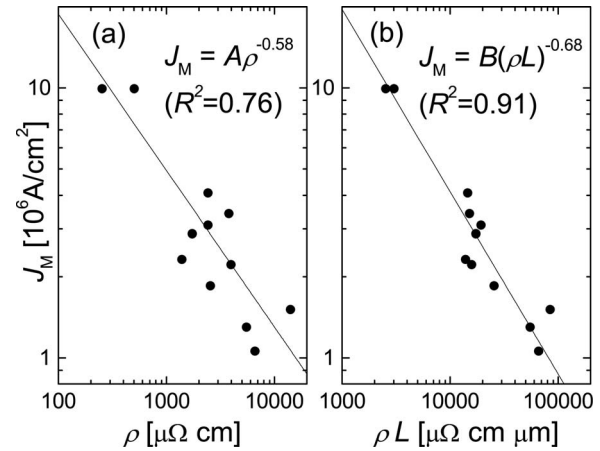


FIG. 5. (a) Resistivity dependence of maximum current density (closed circles). The solid line is a least squares fit using $J_M = A\rho^{-k}$, with $A = 2.7 \times 10^8$ and $k = 0.58$. (b) Maximum current density vs resistivity multiplied by the CNF length (closed circles). The solid line is a least squares fit using $J_M = B(\rho L)^{-n}$, with $B = 2.1 \times 10^9$ and $n = 0.68$. R^2 is the square correlation coefficient of log-log plots.

while the main variation of J_M comes from the variation of ρ as discussed above. This scaling relation is actually deduced by expanding Eq. (3) to the first order of small γ , which corresponds to the weak heat dissipation limit such as our suspended CNF samples in vacuum. The recent work by Tsutsui *et al.*³⁴ proposed similar resistivity-dependent maximum current capacity. In their study, electrical resistivity is defined at low bias region, corresponding to the initial slope of I - V curve. As reasonably pointed out in their paper,³⁴ the I - V curve with positive curvature shown in Fig. 2(c) indicates that the contact resistance of our sample decreases with increasing bias voltage. In this case the initial resistivity mainly comes from the contact, and Eq. (3) does not hold. Instead, the resistivity just prior to the breakdown, which we analyze above, is mostly from CNF and more suitable for the analysis using Eqs. (2) and (3).

The experimentally obtained exponent n indicates that J_M has stronger resistivity dependence than predicted by Eq. (5), corresponding to $n = 0.5$. This means that CNFs with higher resistivity are more prone to failure even at the same generated heat, possibly due to defective morphology such as the inhomogeneous interlayer bonding shown in Fig. 3(a), void creation [Figs. 3(b)–3(d)], or other lattice imperfections. It should be noted that, in multiwalled CNTs, a wall-by-wall breakdown has been observed at constant voltage,¹⁶ inferring that the breakdown of each wall is limited by a similar resistance. This in turn implies that the total current capacity is inversely proportional to resistance, corresponding to $n = 1$, which differs from our result as well. While a more rigorous model to elucidate this dependence is needed, this empirical relation with observable parameters provides a useful guide to improve the current-carrying capacity of CNFs.

V. CONCLUSION

We have studied current-induced breakdown of CNFs with STEM imaging. Cup-shaped failures have been clearly observed, showing that relatively weak interlayer bonding is responsible for breakdown. Weak interlayer bonding also re-

sults in the creation of voids between graphitic layers in the CNF body. Analysis of the maximum current density shows that the mechanism of CNT breakdown can be applied to CNF breakdown with reduced current capacity within and between each graphitic layer. A power law relation between maximum current density and electrical resistivity is observed, demonstrating that the current capacity of CNFs can be improved by lowering electrical resistivity.

ACKNOWLEDGMENTS

The authors are grateful to Kevin Mcilwrath and Konrad Jarausch at Hitachi High-Technologies America, Inc. for their technical support with STEM experiments.

- ¹M. P. Anantram and F. Léonard, *Rep. Prog. Phys.* **69**, 507 (2006).
- ²J. Li, Q. Ye, A. Cassell, H. T. Ng, R. Stevens, J. Han, and M. Meyyappan, *Appl. Phys. Lett.* **82**, 2491 (2003).
- ³F. Kreupl, A. P. Graham, M. Liebau, G. S. Duesberg, R. Seidel, and E. Unger, *Tech. Dig. - Int. Electron Devices Meet.*, 683, 2004.
- ⁴M. Nihei, A. Kawabata, D. Kondo, M. Horibe, S. Sato, and Y. Awano, *Jpn. J. Appl. Phys., Part 1* **44**, 1626 (2005).
- ⁵A. V. Melechko, V. I. Merkulov, T. E. McKnight, M. A. Guillorn, K. L. Klein, D. H. Lowndes, and M. L. Simpson, *J. Appl. Phys.* **97**, 041301 (2005).
- ⁶Q. Ngo, A. M. Cassell, A. J. Austin, J. Li, S. Krishnan, M. Meyyappan, and C. Y. Yang, *IEEE Electron Device Lett.* **27**, 221 (2006).
- ⁷P. Kim, L. Shi, A. Majumdar, and P. L. McEuen, *Phys. Rev. Lett.* **87**, 215502 (2001).
- ⁸Y. Li *et al.*, *Nano Lett.* **4**, 317 (2004).
- ⁹S. Hofmann, G. Csányi, A. C. Ferrari, M. C. Payne, and J. Robertson, *Phys. Rev. Lett.* **95**, 036101 (2005).
- ¹⁰S. Hofmann, C. Ducati, B. Kleinsorge, and J. Robertson, *Appl. Phys. Lett.* **83**, 4661 (2003).
- ¹¹Z. Yao, C. L. Kane, and C. Dekker, *Phys. Rev. Lett.* **84**, 2941 (2000).
- ¹²A. Javey, J. Guo, M. Paulsson, Q. Wang, D. Mann, M. Lundstrom, and H. Dai, *Phys. Rev. Lett.* **92**, 106804 (2004).
- ¹³E. Pop, D. Mann, J. Cao, Q. Wang, K. Goodson, and H. Dai, *Phys. Rev. Lett.* **95**, 155505 (2005).
- ¹⁴P. G. Collins, M. Hersam, M. Arnold, R. Martel, and Ph. Avouris, *Phys. Rev. Lett.* **86**, 3128 (2001).
- ¹⁵B. Bourlon, D. C. Glattli, B. Plaçais, J. M. Berroir, C. Miko, L. Forró, and A. Bachtold, *Phys. Rev. Lett.* **92**, 026804 (2004).
- ¹⁶J. Y. Huang, S. Chen, S. H. Jo, Z. Wang, D. X. Han, G. Chen, M. S. Dresselhaus, and Z. F. Ren, *Phys. Rev. Lett.* **94**, 236802 (2005).
- ¹⁷T. D. Yuzvinsky *et al.*, *Appl. Phys. Lett.* **87**, 083103 (2005).
- ¹⁸J. G. Wen *et al.*, *J. Mater. Res.* **16**, 3246 (2001).
- ¹⁹S. Helveg, C. López-Cartes, J. Sehested, P. L. Hansen, B. S. Clausen, J. R. Rostrup-Nielsen, F. Abild-Pedersen, and J. K. Nørskov, *Nature (London)* **427**, 426 (2004).
- ²⁰H. Cui, X. Yang, M. L. Simpson, D. H. Lowndes, and M. Varela, *Appl. Phys. Lett.* **84**, 4077 (2004).
- ²¹Y. Ominami *et al.*, *Appl. Phys. Lett.* **87**, 233105 (2005).
- ²²Y. Chen, Z. L. Wang, J. S. Yin, D. J. Johnson, and R. H. Prince, *Chem. Phys. Lett.* **272**, 178 (1997).
- ²³Z. F. Ren, Z. P. Huang, J. W. Xu, J. H. Wang, P. Bush, M. P. Siegal, and P. N. Provencio, *Science* **282**, 1105 (1998).
- ²⁴B. A. Cruden, A. M. Cassell, Q. Ye, and M. Meyyappan, *J. Appl. Phys.* **94**, 4070 (2003).
- ²⁵Y. Ominami, Q. Ngo, N. P. Kobayashi, K. Mcilwrath, K. Jarausch, A. M. Cassell, J. Li, and C. Y. Yang, *Ultramicroscopy* **106**, 597 (2006).
- ²⁶L. Zhang, D. Austin, V. I. Merkulov, A. V. Meleshko, K. L. Klein, M. A. Guillorn, D. H. Lowndes, and M. L. Simpson, *Appl. Phys. Lett.* **84**, 3972 (2004).
- ²⁷Y. Qi, T. Çağın, W. L. Johnson, and W. A. Goddard III, *J. Chem. Phys.* **115**, 385 (2001).
- ²⁸H. Cui, O. Zhou, and B. R. Stoner, *J. Appl. Phys.* **88**, 6072 (2000).
- ²⁹See, e.g., B. T. Kelly, *Carbon* **29**, 721 (1991).
- ³⁰K. Mølhave, S. B. Gudnason, A. T. Pedersen, C. H. Clausen, A. Horsewell, and P. Bøggild, *Nano Lett.* **6**, 1663 (2006).
- ³¹C. Durkan, M. A. Schneider, and M. E. Welland, *J. Appl. Phys.* **86**, 1280 (1999).
- ³²M. A. Kuroda, A. Cangellaris, and J.-P. Leburton, *Phys. Rev. Lett.* **95**, 266803 (2005).
- ³³Y.-H. Lee, J.-H. Lee, S. J. Chung, S. Lee, and B. K. Ju, *Appl. Phys. Lett.* **89**, 073109 (2006).
- ³⁴M. Tsutsui, Y. Taninouchi, S. Kurokawa, and A. Sakai, *J. Appl. Phys.* **100**, 094302 (2006).